Acta
Materia
Medica

Research Article

1,7-Bis(4-hydroxyphenyl)-1,4,6-heptatrien-3-one inhibits SARS-CoV-2 by targeting the nucleocapsid protein

Graphical abstract

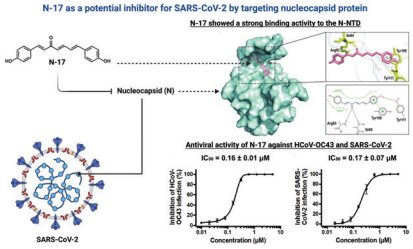

Highlights

- **N-17** is a potential inhibitor of SARS-CoV-2 nucleocapsid protein.
- **N-17** shows nanomolar activity against the HCoV-OC43 and SARS-CoV-2 viruses.
- **N-17** may prevent SARS-CoV-2 replication and transcription by blocking the packaging process of viral RNA.

Authors

Yang Liu, Kuiru Sa, Wei Xu, Yongkang Chen, Jing Liang, Peng Zou and Lixia Chen

Correspondence

zoupeng@shphc.org.cn (P. Zou);
syzyclx@163.com (L. Chen)

In brief

N-17 is a diphenylheptane compound isolated from *Curcuma kwangsiensis*, which exhibits anti-SARS-CoV-2 activity by inhibiting the nucleocapsid protein.

https://doi.org/10.15212/AMM-2023-0021

Acta Materia Medica

Research Article

1,7-Bis(4-hydroxyphenyl)-1,4,6-heptatrien-3-one inhibits SARS-CoV-2 by targeting the nucleocapsid protein

Yang Liu[a,1], Kuiru Sa[a,1], Wei Xu[b,1], Yongkang Chen[b,1], Jing Liang[a], Peng Zou[c,*] and Lixia Chen[a,*]

[a]Wuya College of Innovation, Key Laboratory of Structure-Based Drug Design & Discovery, Ministry of Education, Shenyang Pharmaceutical University, Shenyang 110016, China
[b]Key Laboratory of Medical Molecular Virology (MOE/NHC/CAMS), School of Basic Medical Sciences, Shanghai Institute of Infectious Disease and Biosecurity, Fudan University, Shanghai 200032, China
[c]Shanghai Public Health Clinical Center, Fudan University, Shanghai 201508, China

[1]These authors contributed equally to this work.

***Correspondence:** zoupeng@shphc.org.cn (P. Zou); syzyclx@163.com (L. Chen)

Received: 15 June 2023; Revised: 17 June 2023; Accepted: 18 June 2023

Published online: 7 July 2023

DOI 10.15212/AMM-2023-0021

ABSTRACT

Severe acute respiratory syndrome coronavirus 2 (SARS-CoV-2) has spread globally since 2020. The nucleocapsid (N) protein plays a crucial role in the life cycle of SARS-CoV-2. Here, we established a method to screen inhibitors of N protein by using microscale thermophoresis assays to obtain potential anti-SARS-CoV-2 agents. We identified 1,7-bis(4-hydroxyphenyl)-1,4,6-heptatrien-3-one (**N-17**, a diphenylheptane) as a compound with outstanding inhibitory activity. We further validated the binding of **N-17** to the N-terminal domain of N protein (N-NTD) by using drug affinity responsive target stability assays. We evaluated the ability of **N-17** to bind N protein and predicted the affinity of **N-17** to the N-NTD with molecular docking and molecular dynamics simulation. **N-17** exhibited excellent anti-viral activity against HCoV-OC43 and SARS-CoV-2, with EC_{50} values of 0.16 ± 0.01 μM and 0.17 ± 0.07 μM, respectively. Thus, we discovered a novel SARS-CoV-2 inhibitor targeting the N protein and validated its anti-viral activity *in vitro*. Our results may contribute to the development of promising therapeutic agents for COVID-19.

Keywords: SARS-CoV-2, Anti-viral, N-NTD inhibitor

1. INTRODUCTION

Severe acute respiratory syndrome coronavirus 2 (SARS-CoV-2) has high infectivity and pathogenicity [1]. Although vaccines and some medicines have mitigated the SARS-CoV-2 pandemic [2, 3], the increased infectivity caused by high-frequency genetic mutations in SARS-CoV-2—particularly those in the Omicron variant, which has spread globally—has facilitated viral immune evasion and brought new health risks [4]. Thus, new anti-coronavirus drugs with different mechanisms of action must urgently be developed.

The SARS-CoV-2 genome encodes primarily four structural proteins: the nucleocapsid (N), envelope, membrane and spike proteins. N protein is a multifunctional RNA-binding protein with many critical roles in the formation of helical ribonucleoproteins during the packaging of viral RNA genomes, regulation of viral RNA synthesis in the host and regulation of the metabolism of infected cells [5]. In addition, N protein promotes nuclear factor kappa-B signaling and NLR family pyrin domain containing 3 inflammasome activity in the innate immune system, thereby triggering a "cytokine storm" [6-8]. N protein contains two conserved domains: the nucleocapsid N-terminal domain (N-NTD) and nucleocapsid C-terminal domain (N-CTD) [9]. The N-NTD is responsible for RNA binding, whereas the N-CTD is responsible for dimerization, and both domains contribute to ribonucleoprotein (RNP) formation [10]. Strategies targeting the conserved N protein have shown potential clinical benefits, including attenuating the inflammatory response in hosts infected with SARS-CoV-2 and decreasing SARS-CoV-2 infection [11-13]. Given the importance of the N protein, the N-NTD, which is responsible for RNA binding, may be a key target for drug development.

Discovering therapeutic drugs from naturally occurring compounds is an important strategy for the prevention and treatment of SARS-CoV-2 [14]. Several natural products have been reported to be potential inhibitors of N protein, on the basis of *in silico* screening, such as folic acid, apigenin, catechin, α-spinachsterol, withanolide D, hypericin and silymarin [15-18]. However, most of these inhibitors require further validation of their targeting and inhibitory effects on SARS-CoV-2.

In this study, we purified recombinant N protein expressed in bacteria and used microscale thermophoresis (MST) to screen inhibitors from our own database of natural products. Among the screened compounds, 1,7-bis(4-hydroxyphenyl)-1,4,6-heptatrien-3-one (**N-17**) was identified as a micromolar-level inhibitor. Because of the low yield of **N-17** isolated from *Curcuma kwangsiensis*, we synthesized **N-17** for further research. We subsequently conducted drug affinity responsive target stability (DARTS) assays, molecular docking, molecular dynamics (MD) simulation and *in vitro* anti-viral activity assays. Our findings indicated that **N-17** is a potent N-NTD inhibitor that may serve as a good candidate for SARS-CoV-2 therapy.

2. MATERIALS AND METHODS

2.1 Chemistry

All reagents were procured from commercial sources and used without further purification. Silica gel GF254 and silica gel (200–300 mesh) were used for thin-layer chromatography and column chromatography, respectively. Nuclear magnetic resonance (NMR) spectra were recorded on a Bruker AM-400 spectrometer ($CDCl_3$ = 7.26 ppm for ^1H NMR and 77.16 ppm for ^{13}C NMR, MeOD = 3.31 ppm for ^1H NMR and 49.00 ppm for ^{13}C NMR). Detailed reaction condition information and characterization data are described below.

2.1.1 Synthesis of* (E)*-4-(4-hydroxyphenyl) but-3-en-2-one. The compound 4-hydroxybenzaldehyde (1.74 g, 14.23 mmol) was dissolved in 10 mL anhydrous ethanol, and acetone (15 mL) and 20% NaOH aqueous solution (10 mL) were added in an ice bath. The mixture was then allowed to equilibrate to room temperature and was reacted overnight. After completion of the reaction, the solvent was removed, and the pH was adjusted to neutral with 1 M hydrochloric acid. The aqueous phase was extracted with ethyl acetate, the organic phase was collected and dried, and the crude mixture was purified with silica gel column chromatography (petroleum ether-ethyl acetate = 4:1 (v/v)) with a yield of 80%. ^1H NMR (400 MHz, $CDCl_3$) δ 7.47 (t, *J* = 13.1 Hz, 3 H), 6.88 (d, *J* = 8.6 Hz, 2 H), 6.61 (d, *J* = 16.2 Hz, 1 H), 6.23 (s, 1 H), 2.38 (s, 3 H).

2.1.2 Synthesis of (E)-3-(4-hydroxyphenyl) acrylaldehyde. The compound 4-hydroxybenzaldehyde (312 mg, 0.427 mmol) was dissolved in 5 mL toluene, Wittig reagent (936 mg, 0.512 mmol) was added, and reflux proceeded overnight. The solvent was removed with an evaporator, and the residue was dissolved in ethyl acetate. The residue was then washed three times with saturated salt water, dried with anhydrous Na_2SO_4 and purified with petroleum ether-ethyl acetate = 3:1 (v/v) column chromatography to obtain the intermediate 2, with a yield of 25%.

2.1.3 Synthesis of N-17. Intermediate 1 (220 mg, 1.33 mmol) was dissolved in 10 mL anhydrous ethanol, and intermediate 2 (150 mg, 1.0 mmol) and 20% NaOH aqueous solution (2 mL) were sequentially added to the reaction system in an ice bath. The reaction treatment method was as described for intermediate 1. **N-17** was obtained through silica gel column chromatography with an eluent of petroleum ether-ethyl acetate = 1:1 (v/v), with a yield of 30%. ^1H NMR (600 MHz, MeOD) δ 7.66 (d, *J* = 15.8 Hz, 1 H), 7.58–7.52 (m, 3 H), 7.42 (d, *J* = 8.5 Hz, 2 H), 7.01 (dd, *J* = 15.6, 10.6 Hz, 2 H), 6.93 (dd, *J* = 15.4, 10.8 Hz, 1 H), 6.83 (d, *J* = 8.5 Hz, 2 H), 6.79 (d, *J* = 8.5 Hz, 2 H), 6.65 (d, *J* = 15.1 Hz, 1 H). ^{13}C NMR (150 MHz, MeOD) δ 190.33, 160.21, 158.80, 144.64, 143.67, 142.25, 130.23, 128.79, 127.94, 127.10, 126.30, 123.93, 121.91, 115.54, 115.37. HRMS m/z calcd for $C_{19}H_{17}O_3$ 293.1172, found 293.1178 [M + H^+].

2.2 Biology

2.2.1 Plasmid and reagent details. The human SARS-CoV-2 N-NTD gene cDNA was cloned into the pET-26b (+) vector (Novagen, cat. No. 69862-3) according to information from the N-NTD protein crystal structure (PDB: 6M3M). The gene, primers, and corresponding reagents for N-NTD were provided by Tsingke Biotechnology Co., Ltd. The library of natural small-molecule compounds was derived from previous studies in our laboratory. **N-17**, a typical diphenylheptane, was prepared from *Curcuma phaeocaulis* by our laboratory and identified through comparison of its NMR data (**Supporting Information,** Figure S1–2) with data reported in the literature [19].

2.2.2 Expression and purification of the N-NTD. *E. coli* BL21 was used as the expression strain. The signal clone was pre-cultured at 37°C in 100 mL Luria broth (LB) with kanamycin (35 mg/L) overnight, then transferred into 1 L of LB medium with kanamycin (35 mg/L). Subsequently, 0.4 mM isopropyl-beta-D-thiogalactoside (IPTG) was added until the OD_{600} value reached 0.8. After incubation at 18°C overnight, the bacteria were harvested and centrifuged at 4100 rpm for 10 minutes. The appropriate volume of lysis buffer (50 mM Tris HCl, pH 8.0, 500 mM NaCl and 5 mM β-mercaptoethanol) was used to resuspend the pellet with thorough mixing. The bacteria were disrupted with a Continuous High Pressure Cell Disrupter at 1000 bar for five rounds on ice, then centrifuged at 21500 rpm at 4°C for 30 minutes to remove cell debris. Imidazole solution was added

Acta Materia Medica

to the supernatant to a final concentration of 10 mM. The supernatant was then subjected to gravity column chromatography, and eluted with five to six column volumes of wash buffer (20 mM Tris HCl, pH 8.0, 200 mM NaCl, 10 mM β-mercaptoethanol and 10 mM imidazole) and then five to six column volumes of elution buffer (20 mM Tris-HCl, pH 8.0, 200 mM NaCl, 10 mM β-mercaptoethanol and 150 mM imidazole). The eluted sample was collected and concentrated at 4°C to a volume of approximately 400 μL through ultrafiltration (10 kDa). The resulting protein sample was further purified with a Superdex 200 increase 10/300GL column and AKTA-pure system (GE Healthcare), and eluted with elution buffer (20 mM Hepes, pH 7.5, 200 mM NaCl and 2 mM DTT). The purity of the protein sample was confirmed with 15% SDS-PAGE, and the protein was stored at -80°C.

2.2.3 MST assays. The protein was labeled with a Monolith NTTM Protein Labeling Kit RED (#L001). Compounds were first diluted with labeling buffer (Nano Temper Technologies, Munich, Germany) to a concentration of 20 μM solution with a DMSO content of 8% as the primary screening condition. The equilibrium dissociation constant (K_d) was assessed according to the results of the primary screening. The starting concentration of the tested compound was 10 mM, and fold dilutions were sequentially prepared to obtain a total of 12 concentration gradients. Subsequently, 10 μL of the prepared compound solution was mixed with 10 μL of the diluted protein solution, then incubated at room temperature for 10 min in the dark. Samples were loaded into Monolith standard-treated capillaries, and thermophoresis was performed at 25°C on a Monolith NT.115 instrument (Nano Temper Technologies, München, Germany). The LED power was set to 100%. The analysis software Mo. AffinityAnalysis_X86 was used for data processing, importing microscale thermophoresis curves, and fitting Kd values.

2.2.4 DARTS assays. DARTS assays were performed according to routine procedures, as previously described with some modifications [20]. The N-NTD protein was diluted with saline to 0.2 mg/mL, and the tested compound was dissolved in DMSO to the desired concentration (12.5 μM, 25 μM or 50 μM). The N-NTD protein (39 μL) was incubated with compound solutions at different concentrations for 2 hours at room temperature. Subsequently, 1 mg/mL pronase E solution (5 mg/mL, Sigma-Aldrich) or PBS control was added. After the mixture was incubated at 37°C for 30 minutes, loading buffer (60 mM, pH 8.8, Tris-HCl, 10% SDS, 0.1% bromophenol blue, 25% glycerin and 5% β-mercaptoethanol) was added, and samples were boiled for 5 min. The samples were then separated and analyzed with SDS-PAGE.

2.2.5 HCoV-OC43 and SARS-CoV-2 anti-viral assays. The HCoV-OC43 anti-viral assays were performed according to routine plaque assay procedures, as previously described with some modifications [21, 22]. Briefly, BHK-21 cells were seeded in six-well plates for overnight culture. Subsequently, 100 plaque-forming units of HCoV-OC43 was added to infect cells in the presence of various compound concentrations. After incubation at 33°C for 2 hours, the supernatant was removed, and compounds at different concentrations in DMEM (2% FBS and 1.2% Avicel) were added. After culturing for 3–4 days, BHK-21 cells were fixed and stained with a fixative staining solution (1% crystal violet, 4% formaldehyde and PBS), and the number of plaques was counted after cells were rinsed with water.

To test efficacy against SARS-CoV-2, we performed plaque assays in the Biosafety Level 3 (BSL-3) Laboratory of Fudan University, with similar procedures to those previously described [23]. Vero-E6 cells were first seeded into 96-well plates. After overnight incubation, the compound was serially diluted in DMEM and incubated with authentic SARS-CoV-2 virus for 30 minutes. The mixture was then applied to Vero-E6 and incubated for 2 hours. Subsequently, 1% methylcellulose (Sigma, USA) was added and incubated for 72 hours. Finally, a fixative staining solution was added, and plaques were counted after rinsing with water.

2.3 Cheminformatics

2.3.1 Structure-based molecular docking. The SARS-CoV-2 N-NTD and RNA complex crystal structure (PDB: 7ACT) was obtained from the Protein Data Bank (http://www.rcsb.org). Molecular docking was performed with ICM-Pro 3.8.2 modeling software on an AMD RYZEN 4700 processor (Lenovo, China). The binding pocket was defined according to the literature [24]. The graphical tools in ICM-Pro software were used to expand the binding pocket, and the constructed amino acids of the binding pocket included Thr57, Glu58, Lys61, Arg88, Arg89, Ala90, Thr91, Arg92, Arg93, Ile94, Arg95, Gly96, Gly97, Asp98, Gly99, Lys100, Met101, Lys102, Asp103, Leu104, Ser105, Pro106, Arg107, Trp108, Trp109 and Tyr111. The remaining settings used ICM-Pro default parameters. The PDB (protein) and mol (compounds) files were input into ICM-Pro. The potential energy diagram of the receptor was calculated with default parameters in the docking process, and the ligand with the most reasonable orientation and the lowest energy was selected according to the Monte Carlo procedure [25]. The 2D ligand-protein interaction map was calculated with PoseView in Proteins Plus (https://proteins.plus/), and the 3D interaction map was calculated with PyMOL (The PyMOL Molecular Graphics System, Version 2.6.0a0 Schrödinger, LLC).

2.3.2 MD simulation. The N-NTD-inhibitor complex model (prepared by molecular docking in the previous step) was placed in a TIP3P water box at a minimum distance of 12 Å from each side. The water box was a rectangular cuboid with a volume of 405100.691 $Å^3$. The solvent environment was optimized while the complex

structure was fixed, and then the entire system was optimized. The optimization process consisted of a total of 5000 steps of steepest descent minimization and 5000 steps of conjugate gradient minimization. The entire system was then heated to 300 K in 50 ps under the NVT ensemble with restraintmask the protein and ligand. Subsequently, the systems were equilibrated in 50 ps under the restraints of the NPT ensemble, and another 5 ns equilibration was performed without restraints. Finally, a 65 ns production run was performed at constant temperature (300 K) with other parameters set to default.

MD was performed with the GPU-accelerated version of Amber 22 software [26, 27]. The FF19SB force field was used to treat the protein molecules, whereas the GAFF force field was used to treat the ligand [28-30].

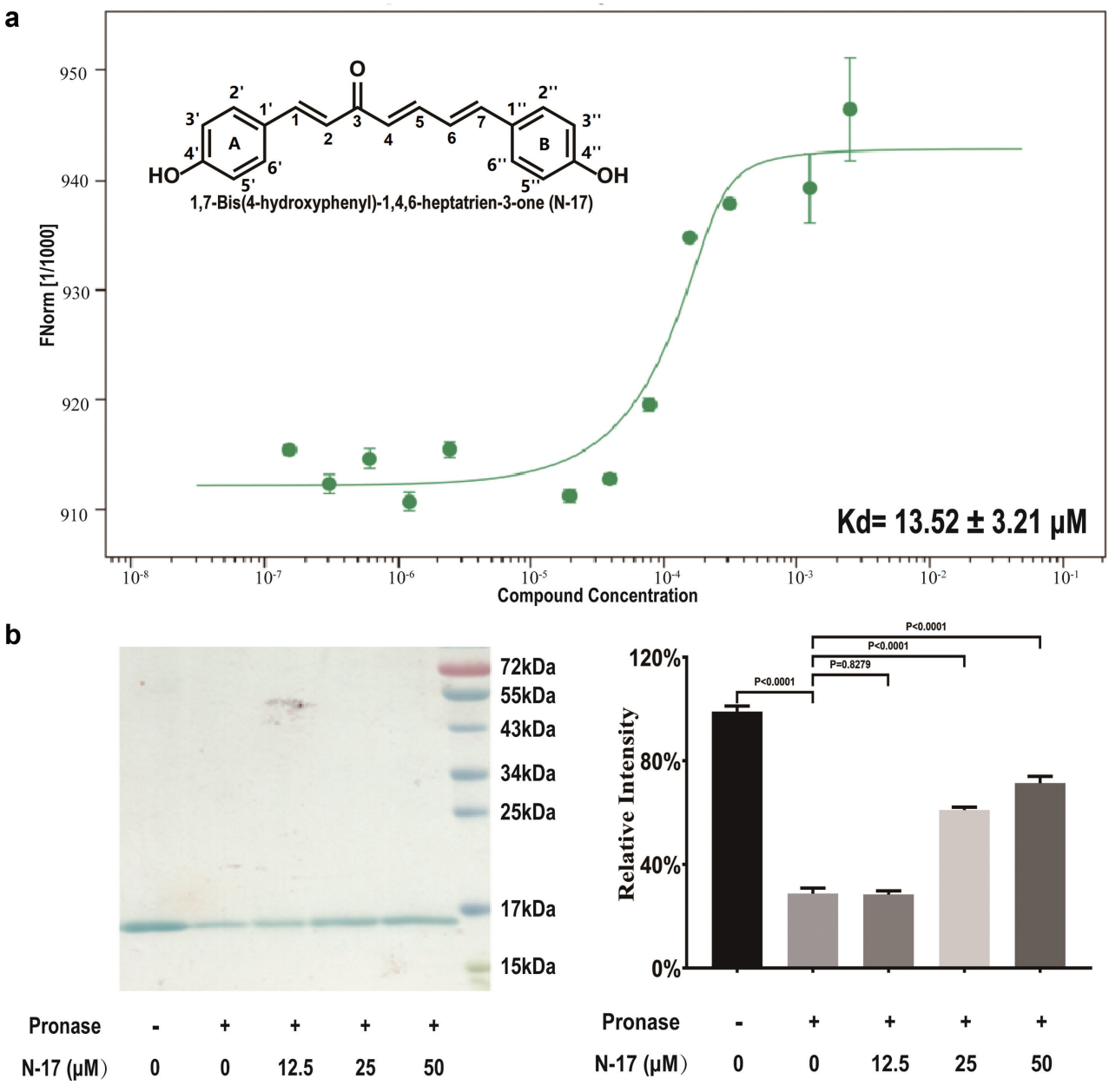

Figure 1 | Binding affinity between N-17 and N-NTD.
(a) Measurement of affinity between the **N-17** and N-NTD by MST. Error bars represent the SD of each data point calculated from three independent thermophoresis measurements, n = 3. (b) **N-17** promotes target-protein N-NTD resistance to proteases, according to DARTS. All data are expressed as mean ± SD, n = 3.

Acta Materia Medica

The geometry optimization (B97-3c) was performed by using ORCA 5.03. ORCA 5.03 and Multifwn 3.8 were used to calculate the RESP2 potential of the ligand [31]. Trajectory analysis was performed with VMD 1.94a57 and CPPTRAJ [32].

2.4 Statistical analysis

All experimental results were obtained through independent experiments with at least three replicates, and the experimental data are presented as mean ± standard deviation (SD). All statistical analyses were performed in GraphPad Prism 8.0 and SPSS 21.0, and *P*-values were determined with Student's t-test.

3. RESULTS

3.1 Identification of N-17 an inhibitor of the N-NTD

We used MST to screen for inhibitors of the N-NTD. MST technology can be used to precisely measure protein-protein or protein-small molecule interactions with low sample consumption, on the basis of fluorescence detection and thermophoresis [33]. Here, we compared the response values of the N-NTD incubated with different compounds with those of the control. The N-NTD and the tested compounds were preliminarily determined to have affinity if the change in

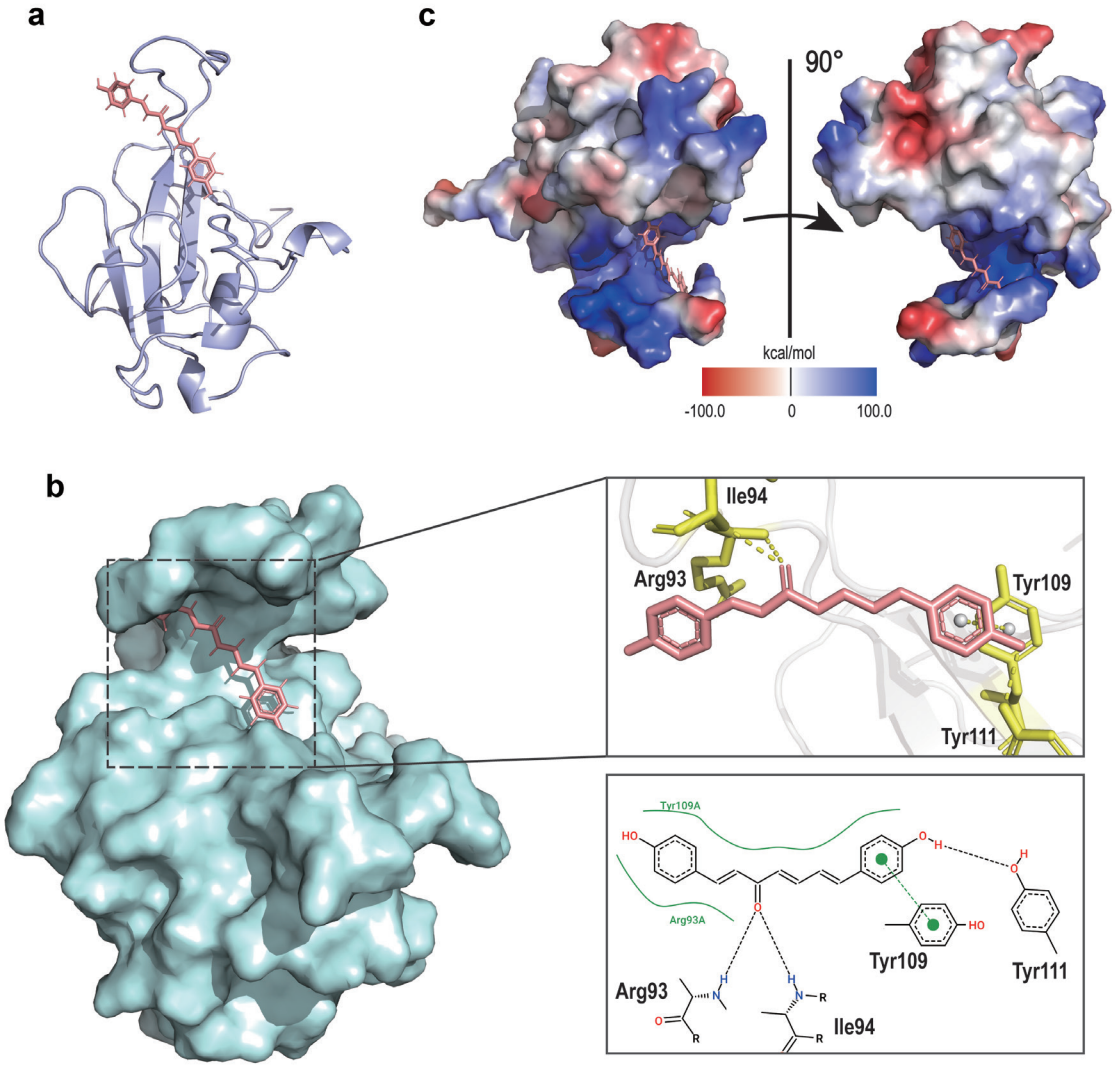

Figure 2 | Protein-ligand interaction model of N-NTD and N-17.
(a, b) Interaction model of N-NTD (PDB: 7ACT) and N-17 in the optimal docking pose. Hydrogen bonds and hydrophobic interactions are indicated by yellow dashed lines, and amino acids involved in these interactions are labeled. (c) Electrostatic surface of the N-NTD-N-17 complex. Blue denotes positive charge potential, whereas red denotes negative charge potential.

thermophoresis value exceeded 10‰. Finally, we screened **N-17** as a compound with strong affinity to the N-NTD. The Kd of **N-17** and N-NTD was determined with MST assays. As shown in **Figure 1a**, the Kd of **N-17** was 13.52 ± 3.21 μM, a value similar to those reported for N protein inhibitors [34], thus demonstrating strong binding affinity of **N-17** to the N-NTD under the tested buffer conditions.

To further verify the interaction of **N-17** with the N-NTD, we performed DARTS assays to monitor target engagement according to the **N-17**-induced stabilization of N-NTD protein. The samples were analyzed with SDS-PAGE and stained with Coomassie brilliant blue. As shown in **Figure 1b**, proteolysis of N-NTD by pronase E clearly decreased after incubation with **N-17** (lanes 3–5) in a concentration-dependent manner, thus suggesting that **N-17** directly binds the N-NTD.

3.2 Molecular docking

To investigate the binding site of **N-17** on the N-NTD, we performed structure-based molecular docking. The N-NTD was found to bind the viral RNA through its positively charged pocket, which has been reported to be composed of Arg92, Arg93, Arg107 and several other residues [24]. As shown in **Figure 2b**, **N-17** fitted well in the binding pocket and formed three hydrogen bonds between the carbonyl at C-3 and Arg93 and Ile94, and between the hydroxyl at C-4″ and Tyr111; in addition, the benzene ring-B formed a hydrophobic interaction with Tyr109. Furthermore, as shown in **Figure 2c**, **N-17** occupied the position of a positively charged gorge in the presumed N-NTD surface electrostatic potential map. Therefore, **N-17** might hinder the binding of N-NTD to RNA and consequently prevent the formation of the SARS-CoV-2 RNP complex.

3.3 MD simulation

To more intuitively explore the binding mode of **N-17** with N-NTD, we applied the protein-ligand 3D structure obtained from the above molecular docking to an MD simulation. Amber 22 was used to perform MD simulation, and the root mean square deviation

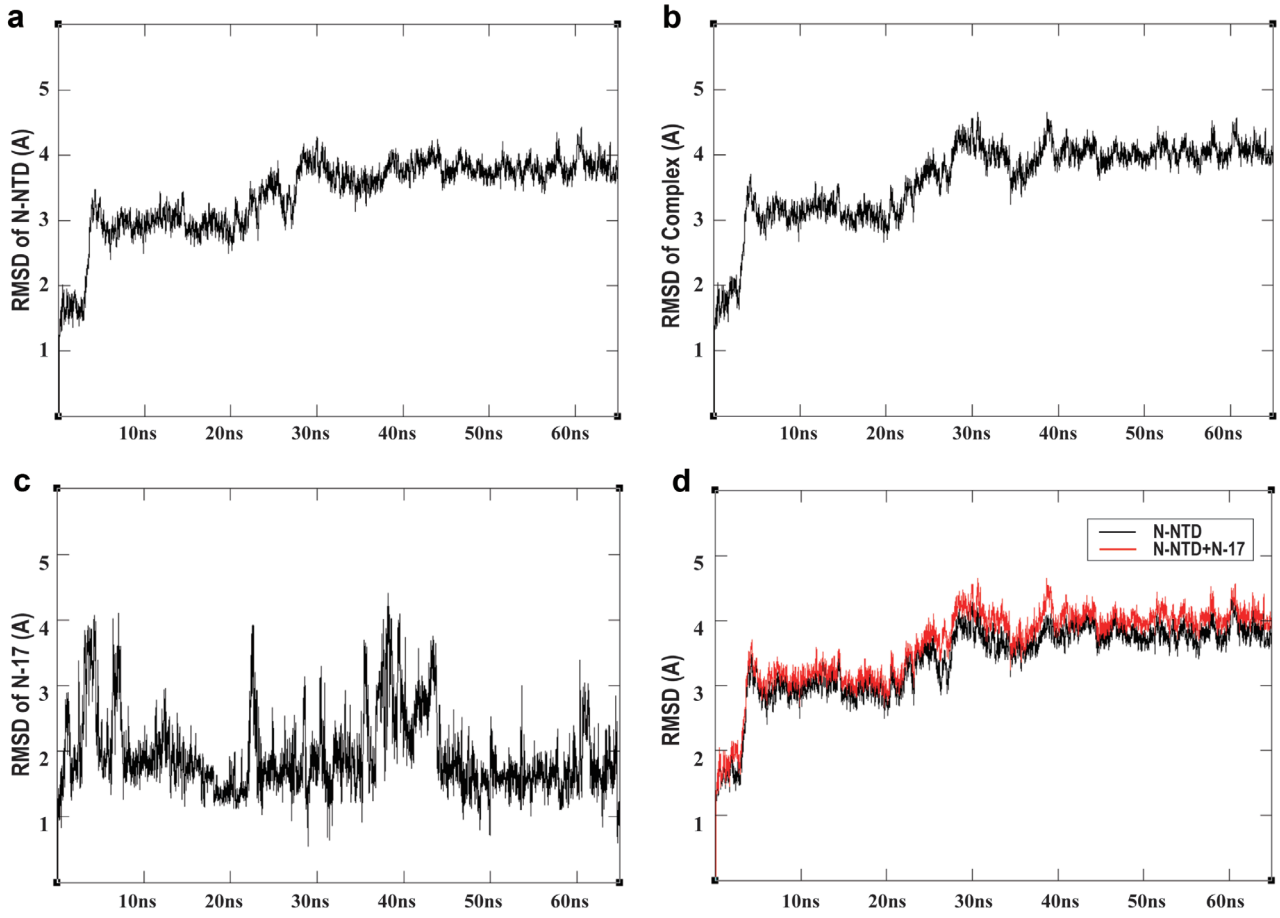

Figure 3 | RMSD between the N-NTD backbone and N-17.
(a) RMSD of the N-NTD. (b) RMSD of the N-17-N-NTD complex. (c) RMSD of N-17. (d) Fusion curves of RMSD plots of N-NTD and the N-17-N-NTD complex.

Acta Materia Medica

(RMSD) was calculated in VMD software. During the simulation process, the stability of the N-NTD backbone and N-NTD-N-17 complex were extensively studied. As shown in Figure 3, the RMSD of the N-NTD and complex remained relatively stable at 30 ns, and was below 3Å. The protein and ligand were bound in a relatively stable manner, thus indicating that **N-17** stably binds the N-NTD.

3.4 Chemical synthesis of N-17

We initially isolated **N-17** from *Curcuma kwangsiensis*, but its low content limited further evaluation of anti-viral activity. Consequently, we referred to the reported three-step chemical method to synthesize **N-17** [35]. First, 4-hydroxybenzaldehyde underwent a condensation reaction with acetone, thus yielding intermediate 1 under alkaline conditions. Subsequently, 4-hydroxybenzaldehyde was converted into intermediate 2 through the Wittig reaction. Finally, intermediate 1 proceeded to an aldehyde-ketone condensation reaction with intermediate 2, thus yielding the final compound (Scheme 1).

3.5 Anti-viral assays

The anti-viral activity of **N-17** toward human β-coronaviruses was assessed. HCoV-OC43, which has low pathogenicity and causes mild respiratory symptoms, is often used to evaluate anti-viral activity. The inhibitory activity of **N-17** against HCoV-OC43 was tested (Figure 4a). At 1 μM concentration, the inhibitory rate of **N-17** toward HCoV-OC43 reached nearly 100%, and its EC_{50} value was 0.16 ± 0.01 μM.

In addition, authentic SARS-CoV-2 was used to evaluate the anti-viral activity of **N-17**. As shown in Figure 4b, the EC_{50} value of **N-17** against SARS-CoV-2 reached 0.17 ± 0.07 μM, thus showing a strong anti-viral effect. This

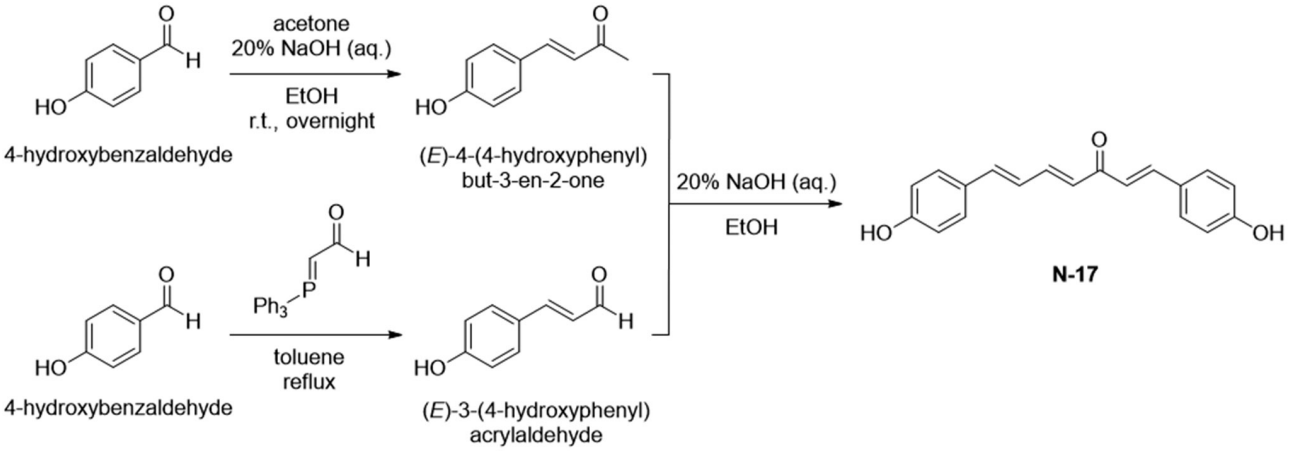

Scheme 1 | Synthesis of N-17.

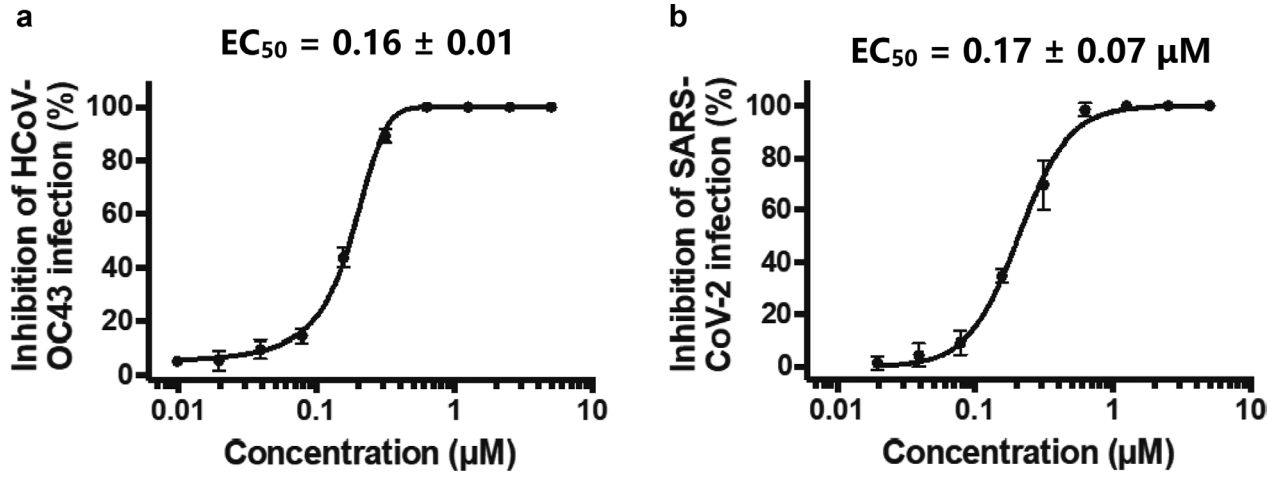

Figure 4 | Anti-viral activities of N-17 against human β-coronaviruses.
(a) Dose-response curves for **N-17** against HCoV-OC43. (b) Dose-response curves for **N-17** against SARS-CoV-2. All data are shown as mean ± SD, n = 3.

nanomolar-level anti-viral activity of **N-17** is a potential natural product, thus supporting potential therapeutic applications for COVID-19.

4. DISCUSSION

The coronavirus pneumonia caused by SARS-CoV-2 infection is highly infectious. The continuing emergence of mutant strains has decreased the protective effects of vaccines and other therapies [36]. Hence, discovering more drugs with better efficacy and safety is crucial.

The selection of drug screening technology is generally based on the affinity between compounds and target proteins, or the effects of compounds on the enzymatic activity of proteins. Because of the lack of a specific substrate for the N-NTD, we decided to use MST to screen for N-NTD inhibitors in this study. Compared with other methods, MST assays do not require immobilization of proteins on an inert surface, and have benefits of low sample consumption and almost no solvent limitations [37]. MST can detect interactions between proteins and their ligands in a highly sensitive manner, thus greatly increasing the precision and confidence of the results, and supporting applications in drug screening.

Some diphenylheptanes have been reported to be potential inhibitors of the main protease, spike glycoprotein and RNA polymerase of SARS-CoV-2, on the basis of virtual screening [38]. Nonetheless, we provide the first demonstration of the inhibitory effect of a diphenylheptane, **N-17**, on the N protein of SARS-CoV-2. According to the formation process of RNPs, two main anti-viral strategies act on N protein: blocking the packaging of viral RNA or inhibiting the oligomerization of N protein [39]. Herein, we demonstrated that **N-17** blocks the packaging process of viral RNA.

Lin *et al.* have proposed several general features for developing coronavirus N-NTD-targeting agents, including the need for a polycyclic aromatic core to achieve π-π stacking with tyrosine residues in the N-NTD [39]. **N-17** contains two benzene rings in its structure; consequently, we observed π-π stacking of phenyl in **N-17** with Tyr109 (**Figure 2b**). Moreover, surface electrostatic potential maps showed that the binding region of **N-17** is mainly in the positively charged region of the N-NTD, and this region tends to be the binding site for RNA [40].

In MST assays, the Kd value of N-NTD and **N-17** was similar to that of another N-NTD inhibitor reported by Luan *et al.*, which has been demonstrated to compete with RNA for N-NTD binding [21]. Therefore, **N-17** was presumed to block binding between N-NTD and RNA, thereby further preventing the replication and transcription of the viral genome. Anti-viral assays in vitro indicated **N-17**'s promising anti-viral activity against SARS-CoV-2, with an EC_{50} value of 0.17 ± 0.07 μM.

Cytokine storm is closely associated with COVID-19 severity and is considered a crucial cause of death due to COVID-19. The high expression of tumor necrosis factor-alpha is a characteristic of the cytokine storm in COVID-19 [41]. **N-17** has been reported to have excellent inhibitory effects on tumor necrosis factor-alpha activity that surpass those of curcumin [42]. Together, the strong anti-inflammatory activity, anti-viral activity *in vitro*, and simple scaffold with outstanding druggability make **N-17** a potential anti-SARS-CoV-2 lead compound, thus suggesting that **N-17** is worthy of further study.

5. CONCLUSION

Herein, we combined MST, DARTS, molecular docking, MD simulation and cell-based anti-viral assays, and identified **N-17**, a diphenylheptane, as a new N-NTD small-molecule inhibitor that blocks RNA binding to the N-NTD and inhibits RNP formation, thus interrupting the SARS-CoV-2 life cycle. Of note, this study provides the first report of a diphenylheptane type compound acting as a SARS-CoV-2 inhibitor targeting the N-NTD. Our findings might guide further studies on anti-coronavirus drugs targeting the N protein.

ACKNOWLEDGEMENTS

We thank the National Natural Science Foundation of China (NSFC) (No. 82141216), Chunhui Program-Cooperative Research Project of the Ministry of Education, Liaoning Province Natural Science Foundation (No. 2022-MS-241) and Shenyang Young and Middle-aged Innovative Talents Support Program (No. RC210446) for financial support. We acknowledge support from the Joint National Local Engineering Research Center of Fujian and Taiwan Chinese Medicine Molecular Biotechnology; Fujian Key Laboratory of Chinese Materia Medica; and Fujian University Key Laboratory for Research and Development of TCM Resources, at Fujian University of Traditional Chinese Medicine.

CONFLICTS OF INTEREST

The authors declare that they have no known competing financial interests or personal relationships that could have appeared to influence the work reported herein.

REFERENCES

[1] V'kovski P, Kratzel A, Steiner S, Stalder H, Thiel V: Coronavirus Biology and Replication: Implications for SARS-CoV-2. *Nature Reviews Microbiology* 2021, 19:155–170.

[2] Pandey SC, Pande V, Sati D, Upreti S, Samant M: Vaccination Strategies to Combat Novel Corona Virus SARS-CoV-2. *Life Sciences* 2020, 256:117956.

[3] Wen W, Chen C, Tang J, Wang C, Zhou M, Cheng Y, et al.: Efficacy and Safety of Three New Oral Anti-viral Treatment (Molnupiravir, Fluvoxamine and Paxlovid) for COVID-19: A Meta-Analysis. *Annals of Medicine* 2022, 54:516–523.

[4] Imai M, Ito M, Kiso M, Yamayoshi S, Uraki R, Fukushi S, et al.: Efficacy of Anti-viral Agents against Omicron Subvariants BQ.1.1 and XBB. *The New England Journal of Medicine* 2023, 388:89–91.

[5] Wang W, Chen J, Yu X, Lan HY: Signaling Mechanisms of SARS-CoV-2 Nucleocapsid Protein in Viral Infection,

Cell Death and Inflammation. *International Journal of Biological Sciences* 2022, 18:4704–4713.

[6] Wu Y, Ma L, Cai S, Zhuang Z, Zhao Z, Jin S, et al.: RNA-Induced Liquid Phase Separation of SARS-CoV-2 Nucleocapsid Protein Facilitates NF-κB Hyper-Activation and Inflammation. *Signal Transduction and Targeted Therapy* 2021, 6:167.

[7] Xia J, Tang W, Wang J, Lai D, Xu Q, Huang R, et al.: SARS-CoV-2 N Protein Induces Acute Lung Injury in Mice via NF-κB Activation. *Frontiers in Immunology* 2021, 12:791753.

[8] Pan P, Shen M, Yu Z, Ge W, Chen K, Tian M, et al.: SARS-CoV-2 N Protein Promotes NLRP3 Inflammasome Activation to Induce Hyperinflammation. *Nature Communications* 2021, 12:4664.

[9] Chen H, Cui Y, Han X, Hu W, Sun M, Zhang Y, et al.: Liquid-Liquid Phase Separation by SARS-CoV-2 Nucleocapsid Protein and RNA. *Cell Research* 2020, 30:1143–1145.

[10] Chang CK, Hou MH, Chang CF, Hsiao CD, Huang TH: The SARS Coronavirus Nucleocapsid Protein--Forms and Functions. *Antiviral Research* 2014, 103:39–50.

[11] Focosi D, Franchini M, Pirofski LA, Burnouf T, Fairweather D, Joyner MJ, et al.: COVID-19 Convalescent Plasma is More than Neutralizing Antibodies: A Narrative Review of Potential Beneficial and Detrimental Co-Factors. *Viruses* 2021, 13:1594.

[12] Herman JD, Wang C, Burke JS, Zur Y, Compere H, Kang J, et al.: Nucleocapsid-Specific Antibody Function is Associated with Therapeutic Benefits from COVID-19 Convalescent Plasma Therapy. *Cell Reports Medicine* 2022, 3:100811.

[13] Dangi T, Sanchez S, Class J, Richner M, Visvabharathy L, Chung YR, et al.: Improved Control of SARS-CoV-2 by Treatment with a Nucleocapsid-Specific Monoclonal Antibody. *Journal of Clinical Investigation* 2022, 132:e162282.

[14] Zhao Y, Deng S, Bai Y, Guo J, Kai G, Huang X, et al.: Promising Natural Products against SARS-CoV-2: Structure, Function, and Clinical Trials. *Phytotherapy Research* 2022, 36:3833–3858.

[15] Chen YM, Wei JL, Qin RS, Hou JP, Zang GC, Zhang GY, et al.: Folic Acid: A Potential Inhibitor against SARS-CoV-2 Nucleocapsid Protein. *Pharmaceutical Biology* 2022, 60:862–878.

[16] Husain I, Ahmad R, Siddiqui S, Chandra A, Misra A, Srivastava A, et al.: Structural Interactions Of Phytoconstituent(s) from Cinnamon, Bay Leaf, Oregano, and Parsley with SARS-CoV-2 Nucleocapsid Protein: A Comparative Assessment for Development of Potential Anti-viral Nutraceuticals. *Journal of Food Biochemistry* 2022, 46:e14262.

[17] Siddiqui S, Upadhyay S, Ahmad R, Gupta A, Srivastava A, Trivedi A, et al.: Virtual Screening of Phytoconstituents from Miracle Herb Nigella Sativa Targeting Nucleocapsid Protein and Papain-Like Protease of SARS-CoV-2 for COVID-19 Treatment. *Journal of Biomolecular Structure and Dynamics* 2022, 40:3928–3948.

[18] Kashyap D, Roy R, Kar P, Jha HC: Plant-Derived Active Compounds as a Potential Nucleocapsid Protein Inhibitor of SARS-CoV-2: An In-Silico Study. *Journal of Biomolecular Structure and Dynamics* 2022, 41:4770–4785. doi: 10.1080/07391102.2022.2072951. Epub ahead of print.

[19] Li W, Wang S, Feng J, Xiao Y, Xue X, Zhang H, et al.: Structure Elucidation and NMR Assignments for Curcuminoids from the Rhizomes of Curcuma Longa. *Magnetic Resonance in Chemistry* 2009, 47:902–908.

[20] Wu Y, Yang Y, Wang W, Sun D, Liang J, Zhu M, et al.: PROTAC Technology as a Novel Tool to Identify the Target of Lathyrane Diterpenoids. *Acta Pharmaceutica Sinica B* 2022, 12:4262–4265.

[21] Chen Y, Wang X, Shi H, Zou P: Montelukast Inhibits HCoV-OC43 Infection as a Viral Inactivator. *Viruses* 2022, 14:861.

[22] Wang X, Chen Y, Shi H, Zou P: Erythromycin Estolate is a Potent Inhibitor against HCoV-OC43 by Directly Inactivating the Virus Particle. *Frontiers in Cellular and Infection Microbiology* 2022, 12:905248.

[23] Liu Z, Xu W, Chen Z, Fu W, Zhan W, Gao Y, et al.: An Ultrapotent pan-β-Coronavirus Lineage B (β-CoV-B) Neutralizing Antibody Locks the Receptor-Binding Domain in Closed Conformation by Targeting its Conserved Epitope. *Protein & Cell* 2022, 13:655–675.

[24] Luan X, Li X, Li Y, Su G, Yin W, Jiang Y, et al.: Anti-Viral Drug Design based on Structural Insights into the N-terminal Domain and C-terminal Domain of the SARS-CoV-2 Nucleocapsid Protein. *Science Bulletin (Beijing)* 2022, 67:2327–2335.

[25] Abagyan R, Totrov M, Kuznetsov D: ICM—A New Method for Protein Modeling and Design: Applications to Docking and Structure Prediction from the Distorted Native Conformation. *Journal of Computational Chemistry* 1994, 15:488–506.

[26] Case DA, Aktulga HM, Belfon K, Ben-Shalom IY, Berryman JT, Brozell SR, et al.: *Amber 2022 Reference Manual*. San Francisco: University of California; 2022.

[27] Salomon-Ferrer R, Götz AW, Poole D, Le Grand S, Walker RC: Routine Microsecond Molecular Dynamics Simulations with AMBER on GPUs. 2. Explicit Solvent Particle Mesh Ewald. *Journal of Chemical Theory and Computation* 2013, 9:3878–3888.

[28] Tian C, Kasavajhala K, Belfon KAA, Raguette L, Huang H, Migues AN, et al.: ff19SB: Amino-Acid-Specific Protein Backbone Parameters Trained against Quantum Mechanics Energy Surfaces in Solution. *Journal of Chemical Theory and Computation* 2020, 16:528–552.

[29] Wang J, Wolf RM, Caldwell JW, Kollman PA, Case DA: Development and Testing of a General Amber Force Field. *Journal of Computational Chemistry* 2004, 25:1157–1174.

[30] Wang J, Wang W, Kollman PA, Case DA: Automatic Atom Type and Bond Type Perception in Molecular Mechanical Calculations. *The Journal of Molecular Graphics and Modelling* 2006, 25:247–260.

[31] Lu T, Chen F: Multiwfn: A Multifunctional Wavefunction Analyzer. *Journal of Computational Chemistry* 2012, 33:580–592.

[32] Humphrey W, Dalke A, Schulten K: VMD: Visual Molecular Dynamics. *Journal of Molecular Graphics* 1996, 14:33–38, 27–28.

[33] Wienken CJ, Baaske P, Rothbauer U, Braun D, Duhr S: Protein-Binding Assays in Biological Liquids using Microscale Thermophoresis. *Nature Communications* 2010, 1:100.

[34] Wang YT, Long XY, Ding X, Fan SR, Cai JY, Yang BJ, et al.: Novel Nucleocapsid Protein-Targeting Phenanthridine Inhibitors of SARS-CoV-2. *European Journal of Medicinal Chemistry* 2022, 227:113966.

[35] Chuprajob T, Changtam C, Chokchaisiri R, Chunglok W, Sornkaew N, Suksamrarn A: Synthesis, Cytotoxicity against Human Oral Cancer KB Cells and Structure-Activity

Relationship Studies of Trienone Analogues of Curcuminoids. *Bioorganic & Medicinal Chemistry Letters* 2014, 24:2839–2844.

[36] Harvey WT, Carabelli AM, Jackson B, Gupta RK, Thomson EC, Harrison EM, et al.; COVID-19 Genomics UK (COG-UK) Consortium: SARS-CoV-2 Variants, Spike Mutations and Immune Escape. *Nature Reviews Microbiology* 2021, 19:409–424.

[37] Moran J, Timon A, Randy W, Heide MR, Stefan D, Philipp B, et al.: MicroScale Thermophoresis: Interaction Analysis and Beyond. *Journal of Molecular Structure* 2014, 1077:101–113.

[38] Zahedipour F, Hosseini SA, Sathyapalan T, Majeed M, Jamialahmadi T, Al-Rasadi K, et al.: Potential Effects of Curcumin in the Treatment of COVID-19 Infection. *Phytotherapy Research* 2020, 34:2911–2920.

[39] Lin SY, Liu CL, Chang YM, Zhao J, Perlman S, Hou MH: Structural Basis for the Identification of the N-terminal Domain of Coronavirus Nucleocapsid Protein as an Anti-Viral Target. *Journal of Medicinal Chemistry* 2014, 57:2247–2257.

[40] Kang S, Yang M, Hong Z, Zhang L, Huang Z, Chen X, et al.: Crystal Structure of SARS-CoV-2 Nucleocapsid Protein RNA Binding Domain Reveals Potential Unique Drug Targeting Sites. *Acta Pharmaceutica Sinica B* 2020, 10:1228–1238.

[41] Hu B, Huang S, Yin L: The Cytokine Storm and COVID-19. *Journal of Medical Virology* 2021, 93:250–256.

[42] Jang MK, Sohn DH, Ryu JH: A Curcuminoid and Sesquiterpenes as Inhibitors of Macrophage TNF-alpha Release from Curcuma zedoaria. *Planta Medica* 2001, 67:550–552.